

# Upscale energy transfer in three-dimensional rapidly rotating turbulent convection

Antonio M. Rubio,<sup>1</sup> Keith Julien,<sup>1</sup> Edgar Knobloch,<sup>2</sup> and Jeffrey B. Weiss<sup>3</sup>

<sup>1</sup>*Department of Applied Mathematics, University of Colorado, Boulder, Colorado 80309, USA*

<sup>2</sup>*Department of Physics, University of California, Berkeley, California 94720, USA*

<sup>3</sup>*Department of Atmospheric and Oceanic Sciences,  
University of Colorado, Boulder, Colorado 80309, USA*

(Dated: August 13, 2013)

Rotating Rayleigh-Bénard convection exhibits, in the limit of rapid rotation, a turbulent state known as geostrophic turbulence. This state is present for sufficiently large Rayleigh numbers representing the thermal forcing of the system, and is characterized by a leading order balance between the Coriolis force and pressure gradient. This turbulent state is itself unstable to the generation of depth-independent or barotropic vortex structures of ever larger scale through a process known as spectral condensation. This process involves an inverse cascade mechanism with a positive feedback loop whereby large-scale barotropic vortices organize small scale convective eddies. In turn, these eddies provide a dynamically evolving energy source for the large-scale barotropic mode. Kinetic energy spectra for the barotropic dynamics are consistent with a  $k^{-3}$  downscale enstrophy cascade and an upscale cascade that steepens to  $k^{-3}$  as the box-scale condensate forms. At the same time the flow maintains a baroclinic convective component with an inertial range consistent with a  $k^{-5/3}$  spectrum. The condensation process resembles a similar process in two dimensions but is fully three-dimensional.

PACS numbers: 47.55.P-,47.27.-i

The evolution of large scale vortex structures from a turbulent state provides a dramatic example of the role played by coherent structures in geophysical flows [1]. In the traditional picture of this process rotation of the Earth is assumed so dominant that vertical motions are strongly suppressed and the flow is modeled by two-dimensional (2D) hydrodynamics [1]. Strongly forced 2D turbulence is dominated by the effects of two inviscid conserved quantities, the energy  $\int_D |\mathbf{u}|^2 dV$  and the enstrophy  $\int_D |\nabla \times \mathbf{u}|^2 dV$  [2]. These conserved quantities are responsible for a downscale enstrophy cascade to small scales where it is dissipated and an upscale energy cascade leading to the appearance of larger and larger scales in the flow [3]. These may be incoherent or organized into coherent structures. In freely decaying flows this process manifests itself in the coalescence of small vortices into larger vortices as the enstrophy decays while the energy remains bounded [4]. In driven flows the large scale structures evolve to ever larger scales until the energy growth in these scales is arrested by physical processes absent from idealized models, e.g., latitudinal variation of the Coriolis force or the presence of Rayleigh friction at the Earth's surface [5]. A similar process arises in wave turbulence and is called spectral condensation [6, 7].

In this Letter we demonstrate the existence of a similar condensation process in three-dimensional (3D) rapidly rotating convection. Fully 3D flows differ from 2D flows by the absence of an enstrophy cascade. In such flows the energy cascade is downscale and in steady state leads to the Kolmogorov  $k^{-5/3}$  energy spectrum [3]. With increasing rotation rate the increasing two-dimensionalization of the flow may therefore lead to a transition from a 3D-like energy spectrum to a 2D-like

spectrum. For this purpose we employ a set of reduced equations describing thermal convection in the rapid rotation limit  $Ro \equiv U/L\Omega \rightarrow 0$ , where  $U$  and  $L$  are the characteristic speed and horizontal scale of the flow, and  $\Omega$  is the local rotation rate. In this limit the flow is locally in geostrophic balance (the Coriolis force is balanced by the pressure gradient at leading order in  $Ro^{-1}$ ), but vertical flows driven by thermal forcing persist at sufficiently small horizontal scales [8, 9]. With a suitable choice of scale and a large enough Rayleigh number measuring the strength of the forcing a statistically stationary state of *geostrophic* turbulence is realized [10, 11].

The development of coherent large scale structures has been observed in experiments on nonrotating isotropic turbulence in thin fluid layers [12–15] and in 2D simulations [16–19]. Simulations in [20] indicate that this is the case in 3D rotating turbulence as well. In this Letter we demonstrate that this process is also present in a convectively forced system, geostrophic turbulence. Specifically, we identify a self-sustaining positive feedback loop between a 2D barotropic (depth-independent) flow and 3D baroclinic (depth-dependent) motion: nonlinear interactions between baroclinic eddies force large-scale barotropic vortical motions, while those between the barotropic and baroclinic components of the flow organize the baroclinic eddies through advection and stretching into a baroclinic state that sustains and enhances the forcing driving the barotropic mode (Fig. 1). These effects grow as nonlinear interactions between the resulting barotropic eddies generate upscale energy transfer from the baroclinic eddy scale to larger scales.

Rapidly rotating Rayleigh-Bénard convection (RRRBC) is described by the non-dimensional

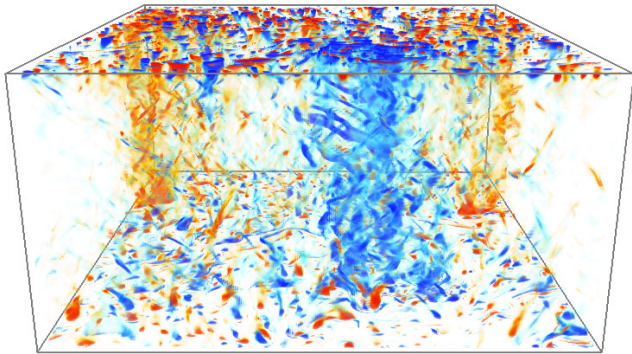


FIG. 1: (color online). Volume rendering of vertical vorticity  $\zeta$  in geostrophic turbulence showing the development of a large scale dipole and the organization of small-scale convective eddies for  $RaE^{4/3} = 100$  and  $\sigma = 1$  at  $t = 100$ .

equations [8–10]

$$\partial_t \zeta + J[\psi, \zeta] - \partial_Z w = \nabla_{\perp}^2 \zeta, \quad (1)$$

$$\partial_t w + J[\psi, w] + \partial_Z \psi = \frac{RaE^{4/3}}{\sigma} \theta + \nabla_{\perp}^2 w, \quad (2)$$

$$\partial_t \theta + J[\psi, \theta] + w \partial_Z \bar{\Theta} = \frac{1}{\sigma} \nabla_{\perp}^2 \theta, \quad (3)$$

$$\partial_{\tau} \bar{\Theta} + \partial_Z (\overline{w\theta}) = \frac{1}{\sigma} \partial_Z^2 \bar{\Theta}, \quad (4)$$

where  $\nabla_{\perp}^2 = \partial_x^2 + \partial_y^2$  and  $J[\psi, f] := \partial_x \psi \partial_y f - \partial_y \psi \partial_x f$  denotes advection with the horizontal velocity  $\mathbf{u}_{\perp} \equiv (-\psi_y, \psi_x, 0)$ . Here  $\psi$  is the pressure,  $\zeta \equiv \nabla_{\perp}^2 \psi$  is the vertical vorticity,  $w$  is the vertical velocity and  $\theta$  is the temperature fluctuation about the mean temperature profile  $\bar{\Theta}$ ; this profile adjusts on the slower time  $\tau = \mathcal{O}(E^{-2/3})$  relative to the  $\mathcal{O}(1)$  convective time  $t$ . The nondimensional parameters are the Rayleigh number  $Ra \equiv g\alpha\Delta T h^3 / \kappa\nu \gg 1$ , Ekman number  $E \equiv \nu / \Omega h^2 \ll 1$ , and Prandtl number  $\sigma \equiv \nu / \kappa = \mathcal{O}(1)$ , where  $\kappa$  and  $\nu$  are the thermal diffusivity and kinematic viscosity,  $g$  is the gravitational acceleration,  $\alpha$  is the coefficient of thermal expansion and  $\Delta T$  is the destabilizing temperature difference between the bottom and the top of the layer. The equations filter out computationally prohibitive fast inertial waves and thin Ekman layers at the top ( $Z = 1$ ) and bottom ( $Z = 0$ ) while capturing geostrophically balanced convective motions on  $\mathcal{O}(E^{1/3})$  horizontal scales. As a result they extend the regime accessible to direct numerical simulation of RRRBC [9, 21, 22].

Equations (1)–(4) were evolved in time for  $Ra = \mathcal{O}(E^{-4/3})$  as described in [9, 10]. We set  $RaE^{4/3} = 100$  and  $\sigma = 1$ , well within the parameter region associated with geostrophic turbulence [9–11]. The spatial domain is periodic in the horizontal, impenetrable in the vertical, and has a nondimensional aspect ratio of  $20L_c \times 20L_c \times 1$ , where  $L_c = 4.8$  is the critical wavelength for linear instability of the conduction state. Wave numbers in the figures are normalized to the box scale  $L \equiv 20L_c$ .

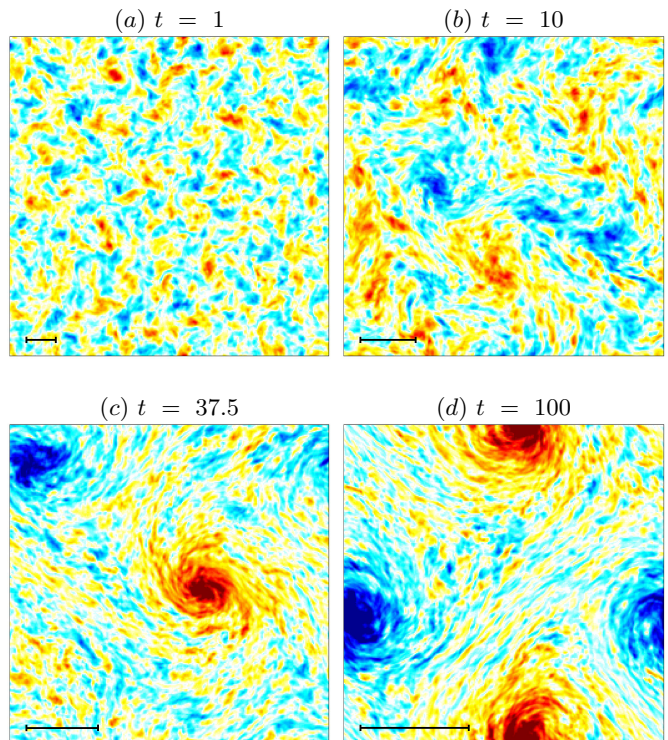


FIG. 2: (color online). Barotropic vertical vorticity at  $t = 1, 10, 37.5,$  and  $100$ , respectively, showing the organization of the flow into structures at progressively larger scales. The black lines indicate one-half wavelength of the dynamically-evolving baroclinic forcing scale  $2\pi/k_f$  defined in the text.

In order to observe the development of the barotropic mode in a controlled fashion the initial condition at  $t = 0$  was generated by starting from an earlier solution that had reached a statistically steady state after numerically suppressing the barotropic vortical mode. The simulation was then restarted and the barotropic mode allowed to evolve freely to study its growth in an otherwise saturated turbulent flow. The growth of the barotropic mode described here occurs on the fast timescale  $t$ , during which the mean temperature profile  $\bar{\Theta}$  remains constant and is robust with respect to changes in the initial condition. Figure 1 shows an example of the large scale dipole structure or condensate that develops in the geostrophic turbulence regime at sufficiently large values of  $Ra E^{4/3}$ . Figure 2 shows the development of this condensate from early to late times. At early times the characteristic scale of the barotropic mode is that of the convective scale  $L_c = L/20$  (panel (a)). After  $t = 10$  the barotropic mode exhibits significant structure at a scale  $\sim L/5$  (panel (b)). By  $t = 37.5$  the barotropic mode has organized into a box-filling dipole (panels (c) and (d)).

To understand the formation of the condensate, Eq. (1) is split into barotropic and baroclinic components. The barotropic component obeys an equation obtained by depth-averaging and noting that  $w = 0$  at the boundaries  $Z = 0, 1$ . The resulting baroclinic vorticity equation

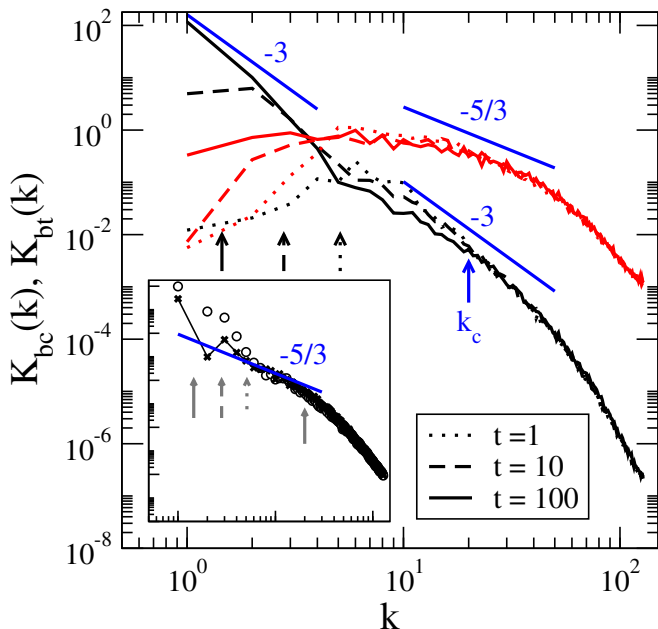


FIG. 3: (color online). Kinetic energy spectra at  $t = 1, 10$  and  $100$  for the barotropic (black lines) and baroclinic (red lines) components. The baroclinic component displays an inertial range  $K_{bc} \sim k^{-5/3}$ . The baroclinic forcing wave number  $k_f$  is indicated by black arrows. The linear instability wave number is  $k_c = 20$ . For small scales  $K_{bt} \sim k^{-3}$ , consistent with a downscale enstrophy cascade; for large scales  $K_{bt}$  steepens to  $K_{bt} \sim k^{-3}$ , consistent with a large-scale condensate. The inset shows an Okubo-Weiss decomposition [23] of  $K_{bt}$  at  $t = 100$  showing that spectral steepening is an effect of the coherent vortex core (o) while the background (x) reflects the incoherent  $k^{-5/3}$  2D upscale energy cascade [2].

(BVE) reads

$$\partial_t \langle \zeta \rangle + J[\langle \psi \rangle, \langle \zeta \rangle] = -\langle J[\psi', \zeta'] \rangle + \nabla_{\perp}^2 \langle \zeta \rangle, \quad (5)$$

where  $\langle f \rangle(x, y) = \int_0^1 f(x, y, Z) dZ$ . Here  $f' \equiv f - \langle f \rangle$  denotes the baroclinic components of the flow. Equation (5) has been studied in detail in the context of forced 2D turbulence [5]. In the absence of viscous diffusion,  $\nabla_{\perp}^2 \langle \zeta \rangle$ , and baroclinic forcing,  $\langle J[\psi', \zeta'] \rangle$ , Eq. (5) conserves area-averaged barotropic energy and enstrophy. We expect therefore an inverse energy cascade within the barotropic mode with a  $k^{-5/3}$  spectrum. We partition the kinetic energy into barotropic and baroclinic components,  $K = K_{bt} + K_{bc}$ , where  $K_{bt} = \frac{1}{2}(\langle u \rangle^2 + \langle v \rangle^2)$  and  $K_{bc} = \frac{1}{2}(u'^2 + v'^2 + w'^2)$ . The growth of barotropic kinetic energy at horizontal wave number  $\mathbf{k}$  obeys

$$\partial_t K_{bt}(\mathbf{k}) = T_{\mathbf{k}} + F_{\mathbf{k}} + D_{\mathbf{k}}, \quad (6)$$

where  $T_{\mathbf{k}} \equiv \sum_{\mathbf{p}\mathbf{q}} T_{\mathbf{k}\mathbf{p}\mathbf{q}}$  and  $F_{\mathbf{k}} \equiv \sum_{\mathbf{p}\mathbf{q}} F_{\mathbf{k}\mathbf{p}\mathbf{q}}$  represent, respectively, the symmetrized transfer of energy between Fourier modes within the barotropic component and the transfer of energy between convective and barotropic modes;  $D_{\mathbf{k}} \equiv -k^2 K_{bt}$  is the viscous dissipation of the

barotropic mode. Moreover,

$$T_{\mathbf{k}\mathbf{p}\mathbf{q}} = b_{\mathbf{p}\mathbf{q}} \text{Re} [\langle \psi_{\mathbf{k}} \rangle \langle \psi_{\mathbf{p}} \rangle \langle \psi_{\mathbf{q}} \rangle] \delta_{\mathbf{k}+\mathbf{p}+\mathbf{q}, \mathbf{0}}, \quad (7)$$

$$F_{\mathbf{k}\mathbf{p}\mathbf{q}} = b_{\mathbf{p}\mathbf{q}} \text{Re} [\langle \psi_{\mathbf{k}} \rangle \langle \psi'_{\mathbf{p}} \psi'_{\mathbf{q}} \rangle] \delta_{\mathbf{k}+\mathbf{p}+\mathbf{q}, \mathbf{0}}, \quad (8)$$

$$b_{\mathbf{p}\mathbf{q}} = b_{\mathbf{q}\mathbf{p}} = \frac{1}{2}(p^2 - q^2)(p_x q_y - p_y q_x), \quad (9)$$

where  $\text{Re}[\dots]$  indicates the real part and  $k \equiv |\mathbf{k}|$  etc. The barotropic fields are functions of horizontal wave number only, while the baroclinic fields in Eq. (8) are functions of the horizontal wave number and height, and then depth-averaged. We shall refer to  $T_{\mathbf{k}}$  as the barotropic cascade and  $F_{\mathbf{k}}$  as the baroclinic forcing. Much work has been done to understand the 2D BVE and  $T_{\mathbf{k}}$  has been well characterized [5, 24, 25]. However, the nature of  $F_{\mathbf{k}}$  for physically realistic forcing and in particular for convective forcing, and its interaction with  $T_{\mathbf{k}}$ , has been heretofore largely unexplored.

Figure 3 shows the spectra of the kinetic energies  $K_{bt}$  and  $K_{bc}$ . The inertial range for the baroclinic component (where energy is the only inviscid invariant) is consistent with the characteristic  $K_{bc} \sim k^{-5/3}$  energy cascade of 3D turbulence downscale from the unstable convective scale  $2\pi/k_c$ . However, the influence of the barotropic dynamics on the baroclinic component is evidenced by the growing power at small wave numbers indicating the genesis of weak large-scale overturning structures which organize the baroclinic eddies. To quantify the time evolution of the baroclinic forcing scale  $2\pi/k_f$  we introduce a threshold scale such that scales smaller than the threshold transfer 75% of the energy from 3D to 2D. Figure 3 (arrows) shows that this scale increases strongly with increasing time.

In contrast, the barotropic kinetic energy displays an inertial range  $K_{bt} \sim k^{-3}$  at scales smaller than  $2\pi/k_c$ , consistent with a downscale enstrophy cascade [2]. At larger scales, the growth of the vortex dipole swamps the expected (incoherent)  $k^{-5/3}$  energy spectrum (Fig. 3, inset); when the dipole reaches the box scale the spectrum steepens to  $K_{bt} \sim k^{-3}$ , as observed in simulations of 2D turbulence [16–19], 3D rotating turbulence at moderate  $Ro$  [20] as well as in experiments on nonrotating turbulence in a thin layer [13].

Figure 4 shows the time evolution of the four largest scales in  $K_{bt}$  along with the total  $K_{bc}$ . One sees that while  $K_{bt}$  grows from zero to an order of magnitude larger than  $K_{bc}$ ,  $K_{bc}$  remains approximately constant, indicating that the baroclinic mode serves as a catalyst for transferring energy from the thermal forcing to the large-scale barotropic flow. Figure 5 shows the corresponding transfer functions  $T_{k\mathbf{p}}$  and  $F_{k\mathbf{p}}$  obtained from the vector transfer functions by integrating over angle and summing over  $\mathbf{q}$ :  $T_{k\mathbf{p}} = \int k d\theta_{\mathbf{k}} \int p d\theta_{\mathbf{p}} \sum_{\mathbf{q}} T_{\mathbf{k}\mathbf{p}\mathbf{q}}$  and similarly for  $F$ . Both  $T$  and  $F$  have also been time-averaged over the spans defined in Fig. 4. Figures 4 and 5 show that at early times,  $t < 1$  (time interval I), the

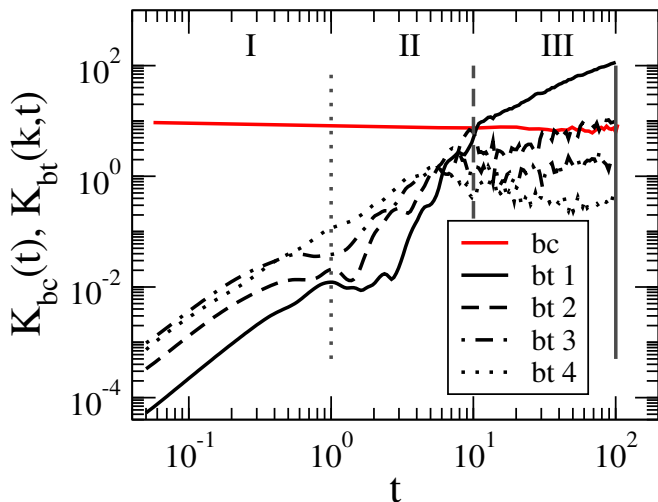


FIG. 4: (color online). The total baroclinic kinetic energy,  $K_{bc}(t)$ , and the kinetic energy  $K_{bt}(k, t)$ ,  $k = 1, 2, 3, 4$ , of the four smallest wave numbers  $k = |\mathbf{k}|$  of the barotropic component. The large scale barotropic energy grows rapidly while the baroclinic energy slowly decreases. Vertical lines define the boundaries of the time intervals used in Fig. 5.

large-scale barotropic modes grow algebraically while the barotropic transfer function  $T_{kp}$  remains negligible, i.e., no barotropic cascade is present, and likewise for the dissipation  $D_k$  (not shown). Thus  $\partial_t K_{bt}(k) \approx F_k$ , where  $F_k \equiv \sum_p F_{kp}$ . One sees that  $F_{kp}$  is large and positive over barotropic wave numbers  $k \in (5, 10)$  and baroclinic catalyst wave numbers  $p \in (5, 10)$ , indicating that the latter are involved in transferring energy from the convective scale to the barotropic component. The baroclinic component has yet to experience the feedback from the growing barotropic component, and  $F_k$  shows that the baroclinic forcing is positive over the range of convectively unstable scales.

During intermediate times,  $1 < t < 10$  (time interval II), a wholly different behavior is observed as  $K_{bt}$  rises to match  $K_{bc}$ . The transfer function for the barotropic cascade,  $T_{kp}$ , acts differently on scales above and below the baroclinic forcing scale. When the wave numbers  $k, p$  are larger than  $k_f$ , the barotropic cascade is localized to the immediate off-diagonal region, where wave numbers  $p \gtrsim k$  put energy into wave number  $k$  while  $p \lesssim k$  take energy out of wave number  $k$ . The net effect seen in  $T_k \equiv \sum_p T_{kp}$  is that the barotropic cascade takes energy out of these wave numbers. For  $k, p$  smaller than  $k_f$  the situation is reversed and the barotropic cascade puts energy into these scales. Overall, the barotropic cascade is an inverse cascade moving energy from small to large scales and generating a largely incoherent  $k^{-5/3}$  spectrum. However, the baroclinic forcing is now significantly changed by the feedback from the barotropic mode leading to increasing coherence. The forcing scale has grown and energy is predominantly put into the barotropic component at large scales ( $k \in (2, 6)$ ) through interaction

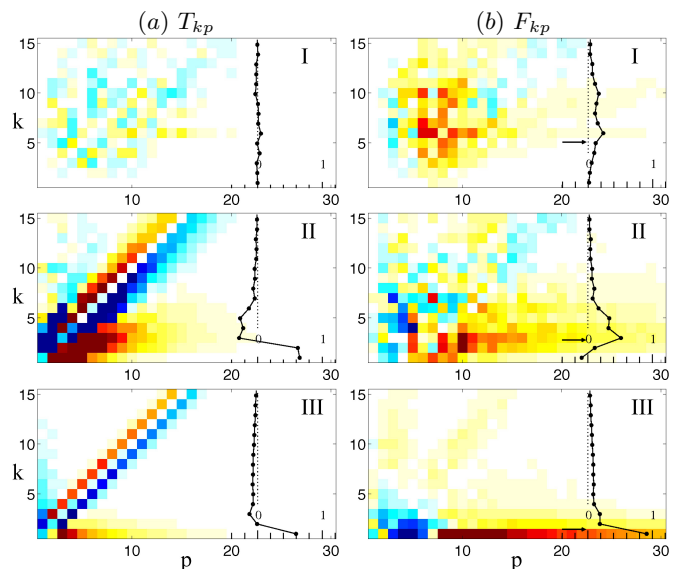


FIG. 5: (color online). Detailed transfer maps,  $T_{kp}$  and  $F_{kp}$ , show how the barotropic self-interaction and the baroclinic-to-barotropic forcing cooperate to move energy to larger scales over the three time intervals identified in Fig. 4 (indicated in the upper right of each panel). Here  $k$  represents the scale at which the barotropic mode is receiving energy and  $p$  is the scale of the catalyst. The color is scaled between  $-0.2$  (blue) and  $0.2$  (red). Sums over  $p$ , i.e., summing over a horizontal line, give  $T_k$  and  $F_k$ , respectively, which are shown as vertical profiles at the right of each panel. In the  $F_{kp}$  panels the black arrows show the approximate forcing scale noted in Fig. 3.

with a broad range of baroclinic catalyst wave numbers  $p \in (2, 16)$ .

At late times,  $10 < t < 100$  (time interval III), the coherent box-scale barotropic mode becomes dominant and the spectrum steepens to  $k^{-3}$ . In this regime the turbulence is constrained by the computational domain and the behavior of the barotropic component resembles the 2D case in which  $\mathbf{u} \cdot \nabla \mathbf{u}$  is balanced by  $\mathbf{u}_t$  resulting in a time-evolving box-scale condensate with  $k^{-3}$  spectrum [17, 26]. The baroclinic forcing is now concentrated in barotropic wave number  $k = 1$  via a very broad range of baroclinic catalyst modes  $p$ . Large baroclinic scales ( $p \lesssim 6$ ) take energy out of the box-scale barotropic mode, while small baroclinic scales ( $p \gtrsim 8$ ) put energy into this mode, the net result being strong positive baroclinic forcing of the box-scale barotropic mode. Apart from this mode all scales have reached a statistically stationary state by  $t = 100$ .

In this Letter we have described the process of spectral condensation in RRRBC and showed that it closely resembles that observed in experiments and simulations of 2D nonrotating turbulence with artificial forcing at an internal scale. Like the 2D Navier-Stokes equation the leading order asymptotic equations (1)–(4) manifest no preference for cyclonic or anticyclonic flow [8, 9]. As a result these equations are ideally suited for studies of spectral condensation in 3D.

This work was supported by the National Science Foundation under FRG grants DMS-0855010 and DMS-0854841. Computational resources supporting this work were provided by the NASA High-End Computing (HEC) Program through the NASA Advanced Supercomputing (NAS) Division at Ames Research Center. One of us (EK) wishes to acknowledge helpful discussions with G. Falkovich and A. C. Newell.

- 
- [1] G. K. Vallis, Atmospheric and Oceanic Fluid Dynamics (Cambridge University Press, Cambridge, U.K., 2006).
- [2] R. H. Kraichnan, *Phys. Fluids* **10**, 1417 (1967).
- [3] U. Frisch, Turbulence: The Legacy of A. N. Kolmogorov (Cambridge University Press, Cambridge, U.K., 1995).
- [4] G. F. Carnevale, J. C. McWilliams, Y. Pomeau, J. B. Weiss, and W. R. Young, *Phys. Rev. Lett.* **66**, 2735 (1991).
- [5] G. Boffetta and R. E. Ecke, *Ann. Rev. Fluid Mech.* **44**, 427 (2012).
- [6] B. Rumpf and A. C. Newell, *Physica D* **184**, 162 (2003).
- [7] C. Connaughton, C. Josseland, A. Picozzi, Y. Pomeau, and S. Rica, *Phys. Rev. Lett.* **95**, 263901 (2005).
- [8] K. Julien, E. Knobloch, and J. Werne, *Theor. Comp. Fluid Dyn.* **11**, 251 (1998).
- [9] M. Sprague, K. Julien, E. Knobloch, and J. Werne, *J. Fluid Mech.* **551**, 141 (2006).
- [10] K. Julien, A. Rubio, I. Grooms, and E. Knobloch, *Geophys. Astrophys. Fl. Dyn.* **106**, 392 (2012).
- [11] K. Julien, E. Knobloch, A. Rubio, and G. Vasil, *Phys. Rev. Lett.* **109**, 254503 (2012).
- [12] J. Sommeria, *J. Fluid Mech.* **170**, 139 (1986).
- [13] H. Xia, H. Punzmann, G. Falkovich, and M. Shats, *Phys. Rev. Lett.* **101**, 194504 (2008).
- [14] H. Xia, M. Shats, and G. Falkovich, *Phys. Fluids* **21**, 125101 (2009).
- [15] H. Xia, D. Byrne, G. Falkovich, and M. Shats, *Nature Physics* **7**, 321 (2011).
- [16] L. M. Smith and V. Yakhot, *Phys. Rev. Lett.* **71**, 352 (1993).
- [17] L. M. Smith and V. Yakhot, *J. Fluid Mech.* **274**, 115 (1994).
- [18] V. Borue, *Phys. Rev. Lett.* **72**, 1475 (1994).
- [19] M. Chertkov, C. Connaughton, I. Kolokolov, and V. Lebedev, *Phys. Rev. Lett.* **99**, 84501 (2007).
- [20] L. M. Smith and F. Waleffe, *Phys. Fluids* **11**, 1608 (1999).
- [21] K. Julien, S. Legg, J. C. McWilliams, and J. Werne, *J. Fluid Mech.* **322**, 243 (1996).
- [22] E. M. King, S. Stellmach, J. Noir, U. Hansen, and J. M. Aurnou, *Nature* **457**, 301 (2009).
- [23] M. Petersen, K. Julien, and J. Weiss, *Phys. Fluids* **18**, 026601 (2006).
- [24] A. Vallgren, *J. Fluid Mech.* **667**, 463 (2011).
- [25] M. E. Maltrud and G. K. Vallis, *Phys. Fluids A* **5**, 1760 (1993).
- [26] C. V. Tran and T. G. Shepherd, *Physica D* **165**, 199 (2002).